Experimental Mechanics (2011) 51:315–334
DOI 10.1007/s11340-010-9362-2

Experimental Investigation on Mechanical Behavior of Coarse Marble Under Six Different Loading Paths

S.Q. Yang · H.W. Jing · Y.S. Li · L.J. Han

Received: 21 October 2009 / Accepted: 11 April 2010 / Published online: 18 May 2010

Abstract A series of triaxial compression experiments were preformed for the coarse marble samples under different loading paths by the rock mechanics servo-controlled testing system. Based on the experimental results of complete stress-strain curves, the influence of loading path on the strength and deformation failure behavior of coarse marble is made a detailed analysis. Three loading paths (Paths I–III) are put forward to confirm the strength parameters (cohesion and internal friction angle) of coarse marble in accordance with linear Mohr-Coulomb criterion. Compared among the strength parameters, two loading paths (i.e. Path II by stepping up the confining pressure and Path III by reducing the confining pressure after peak strength) are suggested to confirm the triaxial strengths of rock under different confining pressures by only one sample, which is very applicable for a kind of rock that has obvious plastic and ductile deformation behavior (e.g. marble, chalk, mudstone, etc.). In order to investigate re-fracture mechanical behavior of rock material, three loading paths (Paths IV–VI) are also put forward for flawed coarse marble. The peak strength and deformation failure mode of flawed coarse marble are found depending on the loading paths (Paths IV–VI). Under lower confining pressures, the peak strength and Young's modulus of damage sample (compressed until post-peak stress under higher confining pressure) are all lower compared with that of flawed sample; moreover mechanical parameter of damage sample is lower for the larger compressed post-peak plastic deformation of coarse marble. However under higher confining pressures (e.g. σ_3=30 MPa), the axial supporting capacity and elastic modulus of damage coarse marble (compressed until post-peak stress under lower confining pressure) is not related to the loading path, while the deformation modulus and peak strain of damage sample depend on the difference of initial confining pressure and post-peak plastic deformation. The friction among crystal grains determines the strength behavior of flawed coarse marble under various loading paths. In the end, the effect of loading path on failure mode of intact and flawed coarse marble is also investigated. The present research provides increased understanding of the fundamental nature of rock failure under different loading paths.

Keywords Coarse marble · Loading path · Strength · Cohesion · Internal friction angle · Flawed sample · Damage sample · Failure mode

S.Q. Yang · H.W. Jing · Y.S. Li · L.J. Han
State Key Laboratory for Geomechanics and Deep Underground Engineering, China University of Mining and Technology, Xuzhou 221008, People's Republic of China

S.Q. Yang (✉) · H.W. Jing
School of Mechanics and Civil Engineering, China University of Mining and Technology, Xuzhou 221008, People's Republic of China
e-mail: yangsqi@hotmail.com

Introduction

All kinds of rock engineering (such deep underground rock engineering, dam-base rock engineering, jointed rock slope project, nuclear waste disposition project, etc.) are usually located in complex triaxial stress state, which is affected by many factors such as different loading path, lithologic character, anisotropy, environment, etc. Since Jaeger [1] pointed out "the possibility of rock failure dependent to the loading path is worth of an argumentative problem" in 1967, the effect of loading path on mechanical behavior of rock has been investigated in past several decades to

understand and explore the fracture mechanism of various rock engineering under different loading paths [2–13]. Up to now, the main experimental results on the influence of loading path on mechanical behavior of rock have included the following three kinds.

- Influence of loading path on the strength and deformation behavior of rock.
- Influence of loading path on the acoustic emission of rock.
- Influence of loading path on failure behavior of rock.

The above first kind of experiment result is widely obtained in previous studies, mainly focusing on the influence of loading path on the strength, volume changes, BDT (brittle-ductile transition) behavior of rock.

On the effect of loading path on strength of rock, there have been two kinds of contradictory opinions. Some typical results were presented as follows. Swanson and Brown [2] investigated the strength of granite under conventional triaxial compression (Path I), confining pressure reduction (Path III) and proportional loading, which showed that strength of granite were independent of the above loading path. Crouch [3] obtained similar conclusion by studying the effect of loading path on the peak strength of norite. However, Xu and Geng [4] studied the various loading paths causing strength, deformation and failure in hard and soft rocks, which found that the effect of two loading paths (Path I and III) on the peak strength was related to lithologic character. The strength of hard rock under Path III was a little lower than that under Path I, but the strength of soft rock under Path III was higher than that under Path I. Wang et al. [5] discussed the effect of Path I and III on the strength parameters of marble, which showed that the peak strength under Path III were all lower than that under Path I and the strength parameters of marble under Path I and III were obviously various. The cohesion of marble under Path III was distinctly lower than that under Path I, but the internal friction angle of marble under Path III had no obvious difference with that under Path I.

On the effect of loading path on deformation behavior of rock, some typical experimental results can be summarized as follows. Gen [6] investigated the volume changes of gabbro and granite under various loading paths, which found that the dilatancy effects of the same rock were quite different in various loading paths. The super-dense and ultra-dilatant states were all observed during testing. Yao et al. [7] carried out the experimental study on BDT of gabbro and marble under two loading paths (Path I and III). Under Path I and III, the gabbro exhibited brittle behavior, but under Path III, the gabbro was more brittle than that under Path I. With the increase of confining pressure, the marble exhibited BDT behavior. But under Path III, some brittle fracture of marble could appear even though under higher confining pressure. Shen et al. [8] performed triaxial test of red sandstone under different loading paths, which analyzed the effect of different loading path on the deformation of rock samples. He concluded that the deformation of rock under different loading paths had nonlinear property, which was unlike the test results under Path I. Xiong and Zhou [9] carried out in-situ true triaxial tests on rock mass under complex loading paths, i.e. (1) σ_1 decreased, σ_2 and σ_3 maintain constant in the same course; (2) σ_1 decreased, σ_2 maintain constant and σ_3 decreased in the same course; (3) σ_1 decreased, σ_2 maintain constant and σ_3 increased in the same course. The results showed that when a principal stress decreased and another one increased in the same process, the deformation was nonlinear and anisotropic. The elastic modulus kept approximately invariable in the loading direction and speed-up decreasing in the unloading direction in accordance with the decreasing of the effective principal stresses.

Besides above experimental results on deformation behaviors under various loading paths, Lee, et al. [10] preformed a series of hollow cylindrical triaxial tests to investigate the potential effect of loading path on the mechanical behavior of the Pei-Tou sandstone, which showed that Kim and Lade's model was shown to be more accurate than the Mohr-Coulomb theory in predicting the failure surface according to the limited test data. Yang et al. [11] investigated the effect of loading path on creep and relaxation behavior of salt rock, which showed that the steady state creep strain rate was strongly dependent on confining pressure in a small range (0~3 MPa), but weakly dependent on loading history. Ferfera et al. [12] carried out the experimental study on monophasic permeability changes under various loading paths to evidence the influence of the effective mean stress and the influence of the deviatoric stress.

Acoustic emission (AE) is a manifestation of releasing the strain energy in the form of elastic wave, which can be used to predict and forecast the failure process of rock engineering and the precursor of earthquake occurrence [14–18]. Chen [15] investigated the influence of two loading paths on the acoustic emission of gabbro and granite under triaxial compression. Under Path I, the average acoustic emission rate gradually increased; while under Path III, an abrupt increase of acoustic emission occurred much later. The total number of acoustic emission events in the fracture process under Path III was much less than that under Path I. The different feature of acoustic emission in various loading modes was due to the existence of the unloading process. Su et al. [16] analyzed the influence of three loading paths (i.e. uniaxial compression, Path I and III) on the acoustic emission of coal sample, which indicated that the AE characteristics of coal sample were different in deformation and failure process under

different loading paths. Compared with Path I, the maximum values of AE counts and energy were much larger, and the results indicated that the failure of coal sample under Path III were more violent. Xiang et al. [17] carried out acoustic emission experimental study of failure process of hard rock under excavating and supporting stress paths. The experimental results indicated that the whole process of AE activity could be divided into three active stages (crevasse crack closing stage, unloading damage stage and destruction stage) and two relatively quiescence stages (elastic stage and fracture stable development stage), which were similar with rock mass behaviors and support effect in project field so as to provide test basis and guide instruction for engineering practice. Li et al. [18] conducted the numerical simulation for the AE behavior of rock by using the RFPA^{2D} (Rock Failure Process Analysis) software to understand the characteristics of Kaiser Effect along different stress paths.

There are less experimental results on the failure behavior of rock under different loading paths, which can be presented as follows. Yao [19] studied the micro-cracks behavior of gabbro under different stress loading paths, i.e. (1) Path I; (2) Path III; (3) Increased the minimum principal stress and kept the rock sample intact (Path A). He observed that there existed obvious differences in micro-fractures between the three paths. Under Path III, most of the micro-cracks in plagioclase were shortened whose lengths were less than the minor axis of the plagioclase grains. These cracks were concentrated in rather narrow regions. Under Path A, the number of inclined micro-cracks increased, and the micro-cracks in the plagioclase grains became much longer and much more in number than that under Path I and III. Zhang et al. [20] adopted rock triaxial test apparatus to model different stress unloading paths according to excavation methods. Five sandstone samples were used to carry out the tests under Path I and III (including confining pressure reduction before peak strength and after peak strength), which showed that the failure under Path III took on brittle failure; moreover the extent of failure of rock under Path III (confining pressure reduction before peak strength) was larger than that under Path III (confining pressure reduction after peak strength). However due to limit experimental results, the above conclusion has still needed to be reinforced.

From above analysis, we can see that up to now, some experiments on the influence of loading path on mechanical behavior of rock have been carried out in previous studies, but the strength, deformation and failure behaviors of rock under various loading paths have not been fully investigated, and the fundamental mechanisms of loading path on the triaxial mechanical behavior of rock are still not fully understood. Besides, real engineering rock mass experienced by loading path is more complex, which makes that mechanical behavior of rock under complex loading paths has been more and more important. Re-fracture mechanical behavior of fractured rock has been one of the most important scientific questions [21–23]. However the re-fracture mechanical behavior of fractured rock is not clear under different loading paths, so it is necessary to explore the mechanical behavior of rock under different loading paths, which is helpful to the effective control of underground engineering rock unstable failure.

Therefore in order to investigate the influence of loading path on mechanical behavior of rock, a number of triaxial compression experiments were carried out for the coarse marble samples under six different loading paths by the rock mechanics servo-controlled testing system. This research is focused on to investigate the influence of loading path on the strength parameters (cohesion and internal friction angle) of coarse marble material, to analyze the re-fracture strength and deformation behavior of flawed and damaged rock sample under different loading paths, and to discuss the failure mode of coarse marble under different loading paths.

Experimental Methodology

Coarse Marble Material and Sample Preparation

In this research, the coarse marble material located the midland ground of China was chosen for the experimental object, which was the same as that in literature [21]. The coarse marble has a crystalline and blocky structure, which is macroscopically very homogeneous with average unit weight about 2700 kg/m^3. The minerals in the coarse marble specimens are mainly calcite, dolomite and magnesite, and the chemical components are mainly Ca and Mg. The crystal size range of the coarse marble is 4.0~6.0 mm (5.0 mm in average). The average crystal size of the coarse marble was determined by optical microscope and SEM.

In order to investigate the mechanical behavior of rock under various loading path, a number of coarse marble samples were prepared to carry out triaxial experiment. When drilling, we machined the coarse marble samples along the same direction in order to avoid the influence of anisotropy on the experimental results of coarse marble. At the same time, machined coarse marble samples were observed and carefully selected to preserve samples suitable for testing. In order to obtain the exact results as well as the best comparison, all the experiments were carried out in natural and dry conditions.

According to the method suggested by the ISRM [24], the length to diameter ratio of tested sample should be in the range of 2.0 to 3.0 in order to minimize the influence of the end friction effects on the testing results. Therefore,

the size of all tested coarse marble samples is cylindrical with 50 mm in diameter and 100 mm in length. As a result, all tested sample with the length to diameter ratio of 2.0 ensure a uniform stress state within the samples. The mechanical behaviors of samples under different loading paths were also determined according to the method suggested by the ISRM.

Testing Procedure for Six Different Loading Paths

All compression experiments for coarse marble samples were carried out on a rock servo-controlled system with the maximum loading capacity of 2000 KN and the maximum displacement capacity of 25 mm. This servo-controlled system can test samples in load or displacement control while the data from LVDT (Linear Variable Displacement Transducer) are recorded and analyzed in real-time.

In this research, we measured the axial force with the loading capacity of 1000 KN and the axial deformation with the displacement capacity of 5 mm. During the whole uniaxial and triaxial compression experiments, loads and deformations of the tested coarse marble samples were recorded simultaneously. Moreover, two rigid steel cylinders (50 mm in diameter and 20 mm in length) were placed between the loading frame and rock sample, which decreased distinctly the influence of the end friction effects on the testing results of marble samples with the length to diameter ratio ~2.0 [25, 26].

In this study, to investigate the effect of the loading path on the strength and deformation failure behavior of coarse marble under conventional triaxial compression, six different loading paths were chosen, which was described in Fig. 1.

Under six different loading paths, the confining pressure is first applied to the sample at a constant rate of 0.5 MPa/s, which ensures that the sample is under uniform hydrostatic stresses ($\sigma_1=\sigma_2=\sigma_3$). And then, the axial deviatoric stress begins to impose the surface of rock sample at the 0.002 mm/s (2×10^{-5}/s) or 0.127 MPa/s control rate. After above procedure, some different loading paths are designed to investigate the effect of loading path on mechanical behavior of coarse marble, which can be seen from Fig. 1.

The above six loading paths in the principal stress space (σ_3, σ_1) are further presented in Fig. 2, in which *oa* and *of* all represent hydrostatic stress ($\sigma_1=\sigma_2=\sigma_3$). *ab*→*bc*, *fg*→*gh* and *ab*→*bh* all represent the loading process under initial confining pressure; *cd* shows the process of confining pressure reduction while keeping axial strain constant; *hi* and *hd* all mean the process of unloading the axial deviatoric stress; *io* represents the process of unloading the confining pressure; *de* and *hg* all mean the process of increasing the confining pressure; *ef* and *gi* all represent the loading process under final confining pressure.

Mechanical Behavior of Intact Sample Under Different Loading Paths (Paths I–II)

Typical axial stress-axial strain curves for intact coarse marble under Path I are shown in Fig. 3, in which the denoted number is the confining stress, MPa. In accordance with Fig. 3, we can conclude that the yielding stress (the stress value that begins to depart the linear elastic phase in the axial stress-axial strain curve) and TCS (triaxial compressive strength) of sample increase gradually with the increase of confining pressure. For intact coarse marble as shown in Fig. 3, the post-peak deformation changes gradually from brittleness to ductility. When σ_3 equals approximately to ~30 MPa, the deformation of the sample comes out distinct yielding platform and the plastic flow takes place, i.e. the post-peak deformation behavior of the sample changes into ideal plasticity [21]. Moreover, in [21], the mechanism on the brittle-ductile transition of intact coarse marble sample has also been made a detailed description.

Taking into account larger plastic and ductile deformation behavior of coarse marble after peak strength, a method of loading path for single sample by Path II is put forward to confirm the peak strength under different confining pressures with only one sample. From Figs. 1 and 2, it is very clear that there is an obvious difference between Path I and II, which can be described as follows. Under Path I, one sample can only confirm a TCS and many samples must be tested to construct the relation between the peak strength and the confining pressure. However under Path II, single sample can be used to obtain a series of TCS. In Fig. 3, the axial stress-axial strain curves of coarse marble under Path II are also shown at two different loading rates, i.e. 0.002 mm/s (2×10^{-5}/s) and 0.127 MPa/s. From Fig. 3, it can be seen that Path II may be used to confirm a series of peak strengths of rock with different confining pressures.

In accordance with the peak strength of intact coarse marble under Path I and II, we can analyze the effect of two loading paths (Path I and II) on the strength behavior by adopting linear Mohr-Coulomb criterion, which can be expressed in terms of the maximum axial supporting capability σ_S and the minimum principal stress σ_3 (i.e. confining pressure) [21], i.e. $\sigma_S=\sigma_0+q\sigma_3$, where σ_0 is usually regarded as UCS (uniaxial compressive strength). The σ_0 and q are related to the cohesion C and the internal friction angle φ, which can be expressed in the following forms, respectively.

$$\sigma_0 = 2C\cos\varphi/(1-\sin\varphi) \tag{1}$$

$$q = (1+\sin\varphi)/(1-\sin\varphi) \tag{2}$$

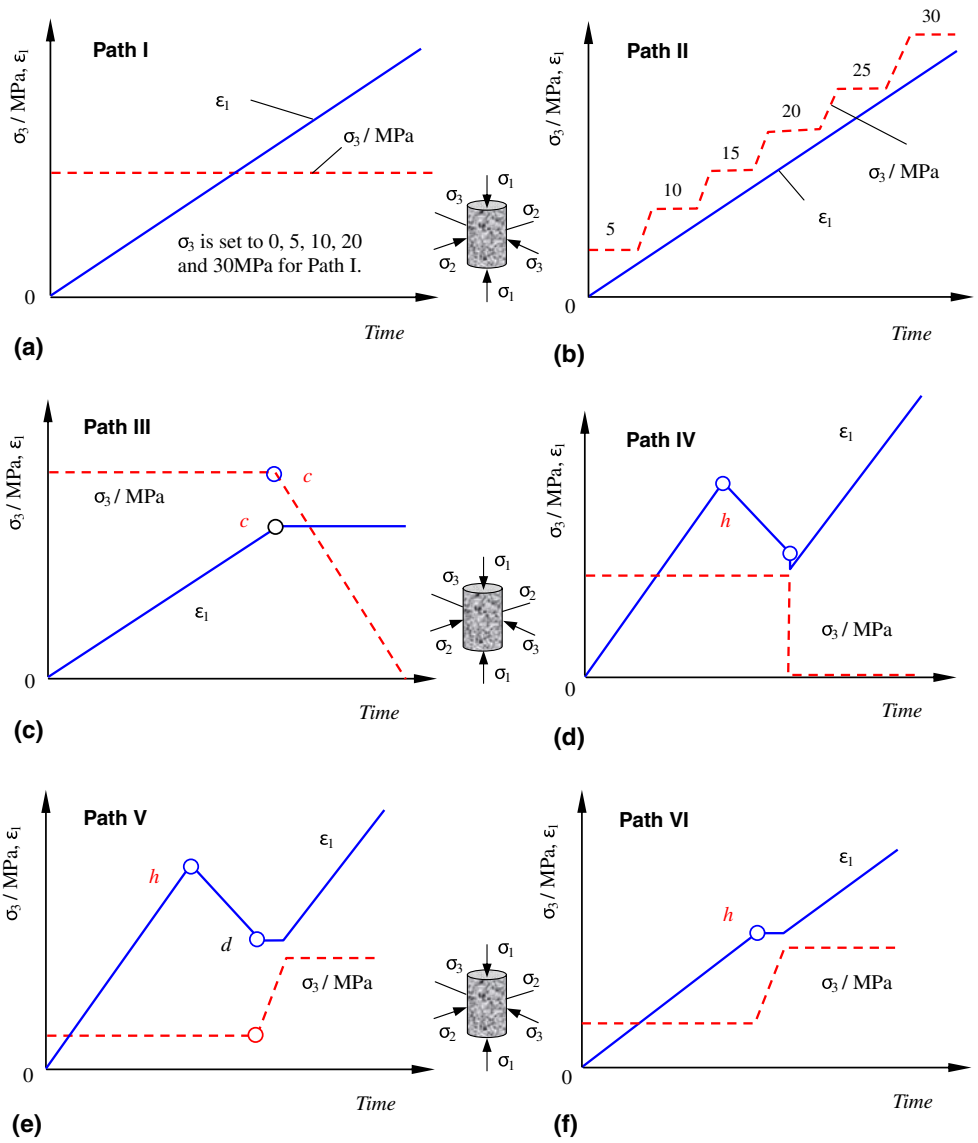

Fig. 1 Six different loading paths in the present study

In accordance with linear Mohr-Coulomb criterion, the influence of σ_3 on σ_S for intact coarse marble sample under Path I and II are presented in Fig. 4. The line $\sigma_S=73.68+2.77\sigma_3$ is regressed according to the strengths of rock obtained under Path I, which there is a good linear regression coefficient of $R=0.985$. It is very clear that the strength of coarse marble sample under Path II has an inappreciable difference with that under Path I, which proves that Path II is very feasible and reasonable to confirm the peak strength of rock under different confining

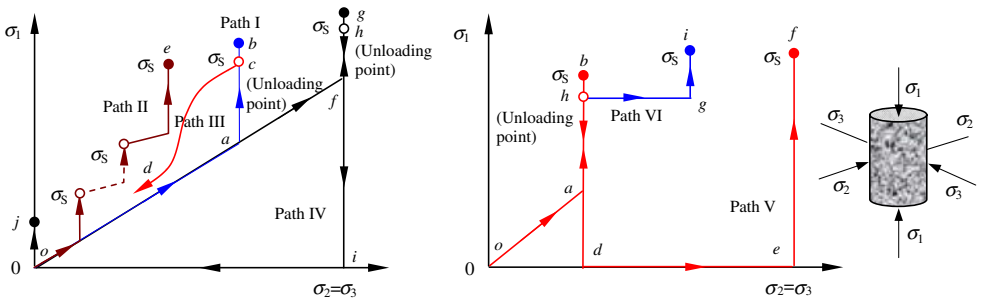

Fig. 2 Six different loading paths presented in the principal stress space (σ_3, σ_1)

Path I: $oa \rightarrow ab$; Path II: oe; Path III: $oa \rightarrow ab \rightarrow bc \rightarrow cd$; Path IV: $of \rightarrow fg \rightarrow gh \rightarrow hi \rightarrow io \rightarrow oj$;
Path V: $oa \rightarrow ab \rightarrow bh \rightarrow hd \rightarrow de \rightarrow ef$; Path VI: $oa \rightarrow ab \rightarrow bh \rightarrow hg \rightarrow gi$;

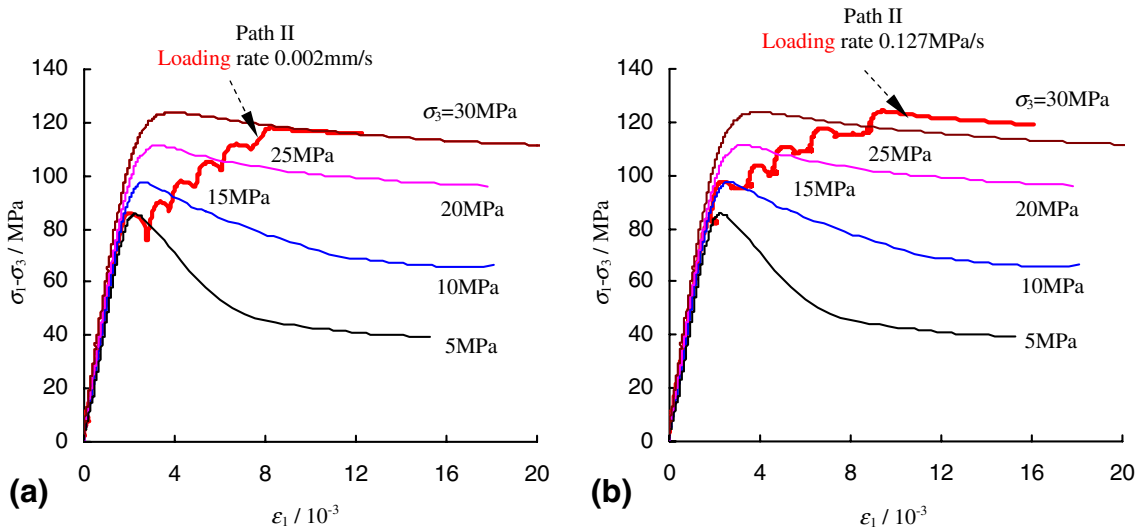

Fig. 3 Typical triaxial stress-strain curves of intact coarse marble under Path I and II (The bold line is the experimental results of coarse marble under Path II; however other experimental results are all obtained under Path I at the loading rate of 0.002 mm/s)

pressures by only one sample. From Fig. 5, we can see out that the intact coarse marble takes on typical shear failure mode even though in uniaxial compression. Therefore, it can be believed that experimental results of intact coarse marble sample have a smaller deviation from the linear Mohr-Coulomb criterion, which testifies that linear Mohr-Coulomb criterion is suitable for intact coarse marble in this research. The intact coarse marble under Path I all lead to typical shear failure mode with a single fracture surface (Fig. 5) and the fracture surface is very smooth, which results from the friction of macroscopic crack surfaces. However the failure mode of coarse marble sample under Path II is similar to that (σ_3=30 MPa) under Path I, as shown in Fig. 5.

Although there are not obvious differences between peak strengths obtained under Path I and II, we can still see out the diversity of peak strengths under Path II at two different loading rates, which is further presented in Table 1. In terms of Table 1, it is very clear that the values of σ_0 and q are 78.35 MPa and 2.32 at a control rate of 0.002 mm/s, while the values of σ_0 and q are 79.28 MPa and 2.55 at a control rate of 0.127 MPa/s. According to equations (1) and (2), it can be seen that, for intact coarse marble sample, the values of C and φ, respectively, equal to 22.14 MPa and 28.0° for Path I; C=25.72 MPa, φ=23.4° for Path II (Loading rate ~0.002 mm/s); and C=24.82 MPa, φ=25.9° for Path II (Loading rate ~0.127 MPa/s), which further illustrates the feasibility and accuracy to confirm the cohesion and internal friction angle of rock by loading Path II with only one sample. It needs to be noticed that suggested rock sample number is not less than five in the ISRM for triaxial compression experiment [24]. However, due to a limited number of cores drilled on-site, especially from weak, stratified and fractured rock mass, moreover testing items are more; it is very difficult to repeat all the experiments in the laboratory. Therefore for a kind of rock that has obvious plastic and ductile deformation behavior (e.g. marble, chalk, mudstone), the Path II are suggested to determine the cohesion and internal friction angle of rock with only one sample, which can eliminate the effect of heterogeneity on the peak strength of rock. But it is not very easy to grasp the control point (A and B shown in Fig. 6) that the axial deviatoric stress is stopped immediately when the sample reaches post-peak stress, which will be explained as follows.

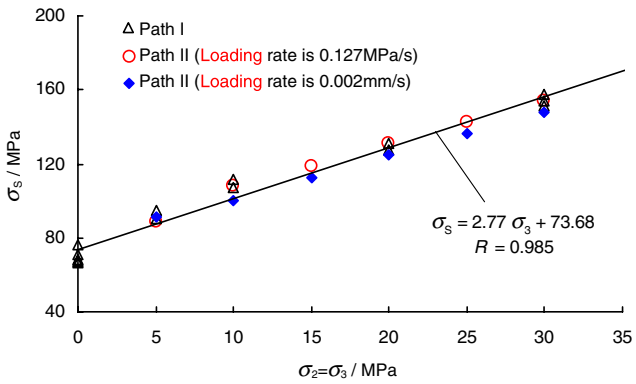

Fig. 4 Strength analysis of intact coarse marble under Path I and II. All the symbols represent the experimental results and the line represents the theoretical value in accordance with Mohr-Coulomb criterion. (R is the correlation coefficient of determination of the regression)

Figure 6 shows the axial stress-axial strain curves of intact coarse marble under Path I and II. At σ_3=5 MPa, the strength and deformation behavior of three different samples have a good consistency. The maximum difference of peak strength is only 2.55 MPa, which can be seen from

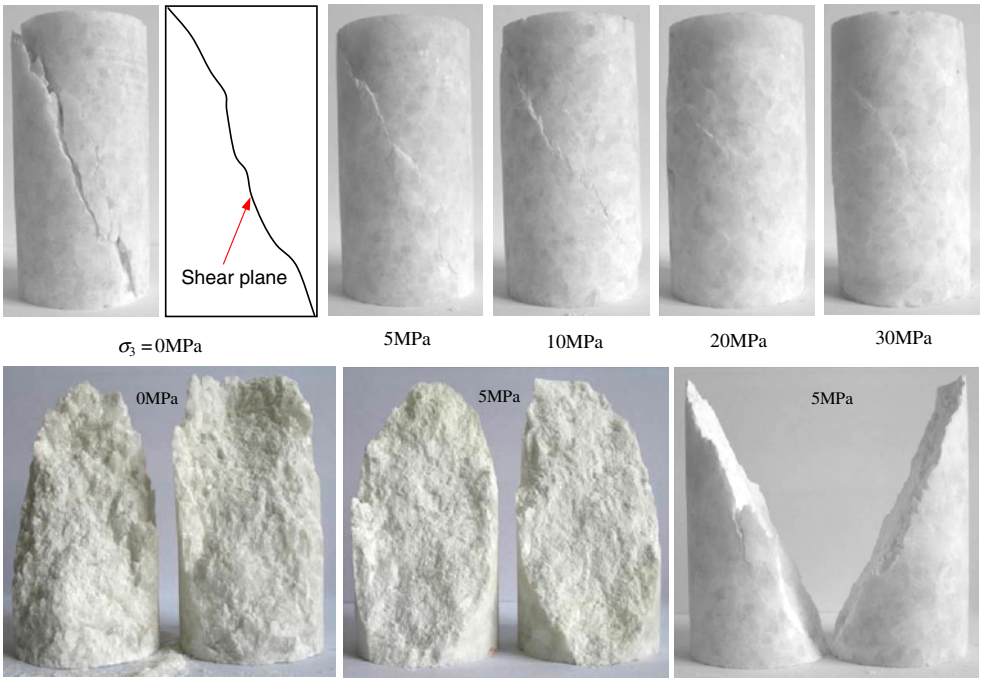

Fig. 5 Failure modes of intact coarse marble under different confining pressures (Path I)

Fig. 6. However, from Fig. 6, we can conclude that the difference of peak strength between two different loading rates besides σ_3=5 MPa all reach 6.0 MPa (Fig. 4), which results from the following possibilities:

(1) Heterogeneity of rock material, which reflects the difference among different samples;
(2) Effect of loading rate on the peak strength;
(3) The difference among damage samples loaded to post-peak stress (i.e. control point *A* and *B*).

From Fig. 6(a) and (b), it is easy to see out that the smaller effect of the above first and second reason on the peak strength of intact coarse marble, which the maximum influence is not more than 2.55 MPa. Therefore the third reason is very significant on the peak strength of intact coarse marble. At the loading rate of 0.127 MPa/s, the sample C13$^{\#}$ was loaded up to *B*-point; while at the loading rate of 0.002 mm/s, the sample C10$^{\#}$ was loaded up to *A*-point. Therefore the difference between C10$^{\#}$ and C13$^{\#}$ samples that is applied respectively to control point *A* and *B* are very distinct, the C10$^{\#}$ sample has more damage than the C13$^{\#}$ sample after loading to control point at σ_3=5 MPa, which results in the difference of peak strength as shown in Fig. 6. Moreover the difference of peak strength at two loading rates is almost in-dependent to the confining pressure higher than 5 MPa. Therefore it is very important to grasp accurately the control point (*A* and *B* shown in Fig. 6) for confirming the strength parameters by the loading path of stepping up the confining pressure with only one sample (Path II).

Table 1 Effect of loading path on strength parameters of intact coarse marble in accordance with linear Mohr-Coulomb criterion

Loading path	Loading rate	σ_0 / MPa	q	C / MPa	φ / (°)	R
Path I	0.002 mm/s	73.68	2.77	22.14	28.0	0.985
Path II	0.002 mm/s	78.35	2.32	25.72	23.4	1.000
	0.127 MPa/s	79.28	2.55	24.82	25.9	0.995

All the experiments in Table 1 were all carried out in January, 2007

Mechanical Behavior of Flawed Sample Under Different Loading Paths (Paths III–VI)

In this section, the flawed coarse marble was chosen as the research object. By analyzing the re-fracture behavior of flawed sample under four different loading paths (Paths III~VI), we tried to reveal the re-fracture deformation mechanism of flawed sample. Table 2 lists re-fracture strength behavior of flawed coarse marble under different loading paths (Paths III~VI). σ_3^i represents the initial confining pressure; σ_S^i represents the maximum axial supporting capability at σ_3^i. While σ_3^f and σ_S^f, respectively, represents the final confining pressure and the final maximum axial supporting capability. All the above parameters were denoted by Fig. 7. Figure 7 shows experimental results on change of the confining pressure, axial deviatoric stress, axial strain of coarse marble with the increase of time under Path IV, which is approximately same compared with Fig. 1(d).

Figure 8 shows triaxial stress-strain curves of flawed coarse marble at initial confining pressures with different

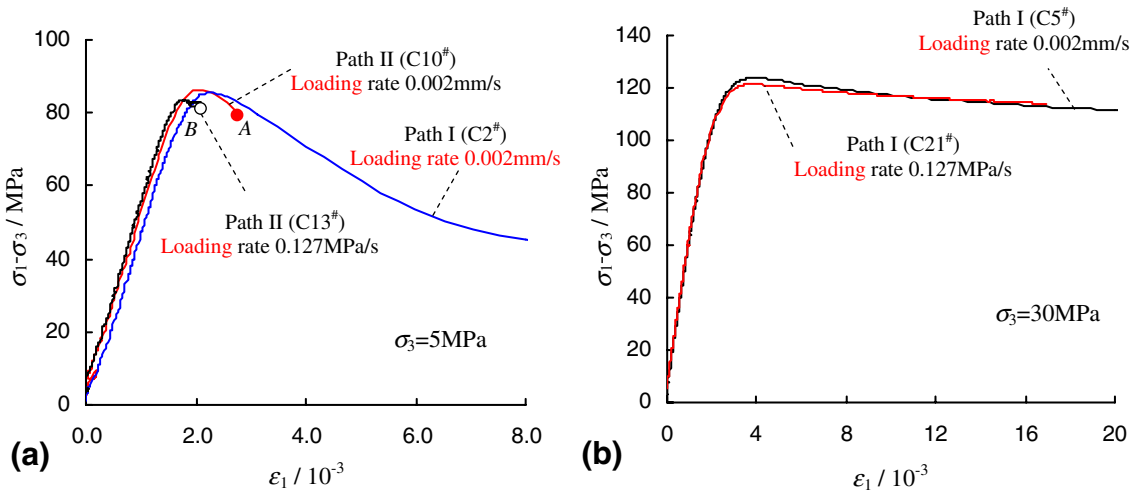

Fig. 6 Axial stress-axial strain curves of intact coarse marble under Path I and II (σ_3=5 MPa and 30 MPa)

loading paths. Although in this research all the coarse marble samples under Paths I~VI were machined from the same block along the same direction, the experimental coarse marble still shows two kinds of different mechanical behaviors due to the difference of experimental date. In order to distinguish the difference, under Paths I~II, tested samples were all called "intact sample"; while under Paths III~VI, test samples were all called "flawed sample". It needs to notice that "flawed sample" in this research is distinctly different from that with pre-existing cracks in [21, 23].

From Fig. 8, we can conclude that the flawed samples fail with smaller Young's moduli and larger failure strains compared with intact samples at the same confining pressure. At lower confining pressures (≤10 MPa), an interest experiment phenomenon for flawed coarse marble was observed as follows. All the axial stress-axial strain curves of flawed samples show a turning point (an abrupt change of slope) at the deviatoric stress of about 35 MPa, coincident with local yield in the coarse marble. For flawed samples, except for C15#, C22#, C24# and C26# samples (Table 2 and Fig. 8), the local yield extent of other flawed samples are all approximately equal. From Fig. 8(a), it can be seen that local yield extent of C24# and C26# samples are larger than that of C16# and C31# samples, which results in smaller Young's moduli, larger failure strains and lower strengths of C24# and C26# samples. Moreover C24# and C26# samples have more plasticity after peak stress than that of C16# and C31# samples. Under highest confining pressure of 30 MPa, the axial stress-axial strain curve of flawed sample C27# does not show a turning point at the deviatoric stress of 35 MPa, which results from the occurrence of local yield under hydrostatic stress of 30 MPa. The above analysis reflects the effect of confining pressure on the local yield, while, the confining pressure does not have a distinct influence on the Young's modulus after turning point, which can be seen from Fig. 8(d). For flawed sample, except for four samples (C15#, C22#, C24#

Table 2 Initial and re-fracture strength behavior of flawed coarse marble under different loading paths (Paths III–VI)

Sample	D/mm	L/mm	Loading path	Flawed extent / δ	σ_3^i/MPa	$\sigma_S^i - \sigma_3^i$/MPa	σ_S^i/MPa	σ_3^f/MPa	$\sigma_S^f - \sigma_3^f$/MPa	σ_S^f/MPa
C7#	49.7	100.8	III	0.265	30	135.97	165.97	Reducing confining pressure after peak strength		
C14#	49.7	100.1	IV	0.311	30	133.19	163.19	0	49.94	49.94
C27#	49.7	100.2	IV	0.327	30	132.22	162.22	0	38.37	38.37
C15#	49.7	99.4	V	0.697	3	59.44	62.44	30	124.52	154.52
C22#	49.7	99.9	V	0.658	5	70.14	75.14	30	124.70	154.70
C19#	49.7	99.5	V	0.526	10	97.95	107.95	30	129.16	159.16
C16#	49.7	99.8	VI	0.424	5	80.69	85.69	10	71.29	81.29
C24#	49.7	99.8	VI	0.643	5	70.04	75.04	20	101.52	121.52
C31#	49.7	99.8	VI	0.518	5	80.97	85.97	20	103.21	123.21
C26#	49.7	101.0	VI	0.614	5	68.04	73.04	30	122.91	152.91

All the experiments in Table 2 were all carried out in July, 2009

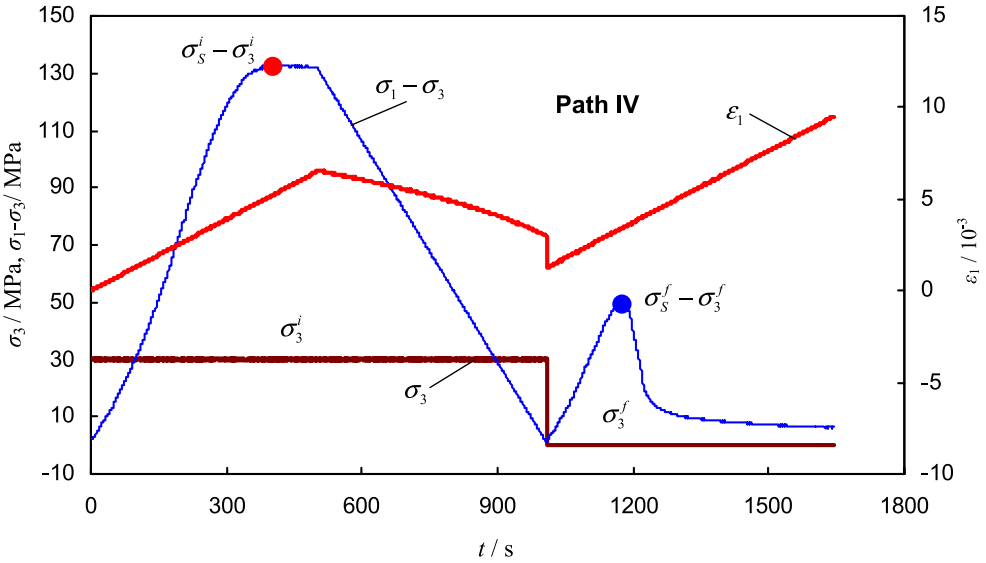

Fig. 7 Experimental results on change of confining pressure, axial deviatoric stress, axial strain of coarse marble with the increase of time under Path IV, which is approximately same compared with Fig. 1(d)

and C26#), we can conclude that the Young's modulus of flawed sample is in-dependent to the confining pressure; if not taking into account the effect of turning point on the stress-strain curve, the Young's moduli of other flawed samples are approximately equal [Fig. 8(d)]. From the stress-strain curve of C22# and C24# samples, we can see that the flawed sample C22# have larger plastic deformation after unloading, but it is very clear that two cycle loading-

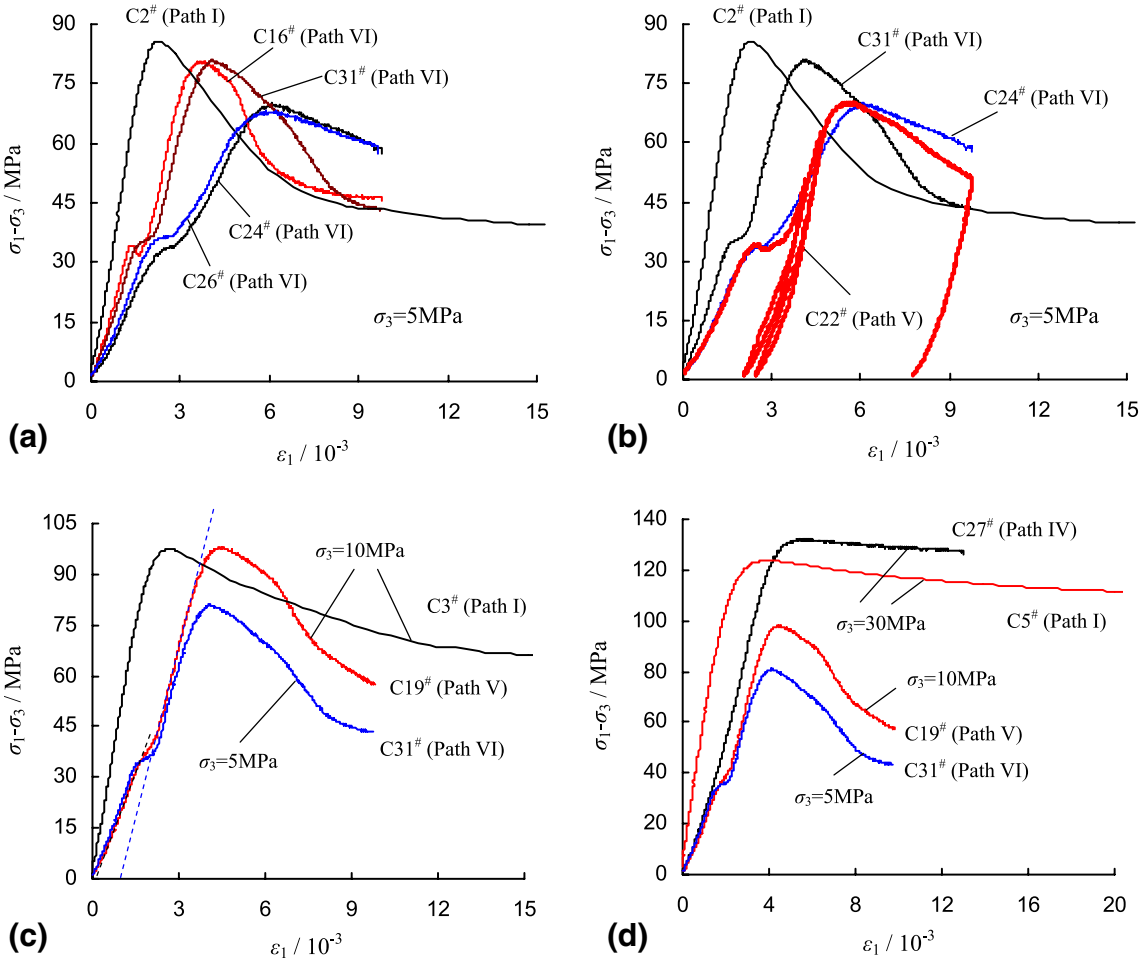

Fig. 8 Triaxial stress-strain curves of flawed coarse marble at initial confining pressures with different loading paths. Under Paths I~II, tested samples were all "intact sample"; while under Paths III~VI, test samples were all "flawed sample"

unloading do not increase the peak strength of flawed sample, while increase the slope of axial stress-axial strain curve after turning point.

From Table 2 and Fig. 8, the following conclusions can also be found out for all the flawed samples. Under lower confining pressures (e.g. 5 MPa), the peak strength of flawed sample is lower than that of intact sample. Under medium confining pressures (e.g. 10 MPa), the peak strength of flawed sample is approximately equal to that of intact sample. However under higher confining pressures (e.g. 30 MPa), the peak strength of flawed sample is higher than that of intact sample. The above conclusion can be explained as follows. Confining pressure has a key effect on the local yield in the rock material. With the increase of σ_3, the local yield will take place in advance. And thus the material in the rock extrudes and fractures after local yield, which fills in the internal voids of flawed sample and strengthens the supporting structure in the rock material. But with the increase of σ_3, this kind of strengthening will become more and more distinct, which can increase the elastic modulus of flawed sample after turning point, as shown in Fig. 8(c). Therefore the difference on peak strength of between flawed and intact sample increases with the increase of σ_3.

For the flawed extent of coarse marble, in fact it is very difficult to make a quantitative definition because rock is a kind of natural geological material, and is strongly heterogeneous at the three-dimensional (3-D) mesoscopic scale. Up to now, there has still not been a kind of good way to measure the flawed extent in the rock material. Therefore, in this research, the following method (i.e. flawed extent δ) is put forward to discuss and provide approximately a quantitative definition for the flawed extent of coarse marble.

Flawed extend :

$$\delta = \frac{E_{Sintact} - E_{Sflawed}}{E_{Sintact}} = 1 - \frac{E_{Sflawed}}{E_{Sintact}} \tag{3}$$

Where, $E_{Sintact}$ and $E_{Sflawed}$ is respectively defined as the elastic modulus of intact and flawed sample, which are listed in Fig. 9. The elastic modulus is defined as the slope of approximation linear part in the axial stress-axial strain curve. For flawed sample, the stress-strain curve before turning point is adopted to calculate the elastic modulus. From Fig. 9, on the whole, the elastic modulus of intact and flawed coarse marble all increase with the confining pressure. In accordance with equation (3), the values of δ are listed in Table 2 and the relation between δ and σ_3 is plotted in Fig. 9(b). From Fig. 9(b), we can see that the flawed extent δ is not a constant, which varies with heterogeneity of rock material and confining pressure. The average value of δ of four samples (C15$^{\#}$, C22$^{\#}$, C24$^{\#}$ and C26$^{\#}$) is ~0.653, and the dispersion extent is about 12.7%. The average value of δ of three samples (C19$^{\#}$, C31$^{\#}$ and C16$^{\#}$) is ~0.489, and the dispersion extent is about 20.9%. However, at the confining pressure of 30 MPa, the average value of δ of three samples (C7$^{\#}$, C14$^{\#}$ and C27$^{\#}$) is 0.301, and the dispersion extent is about 20.6%. The above description shows that the flawed extent δ is not a static parameter but a dynamic parameter, which decreases with the increase of confining pressure as shown in Fig. 9(b).

Mechanical Behavior of Flawed Sample Under Reducing the Confining Pressure (Path III)

Triaxial experimental results of flawed coarse marble under Path III are shown in Fig. 10. From Fig. 10(a), it can be seen that the confining pressure is reduced after applying to post-peak stress for the sample under Path III, which is different from the confining pressure reduction before peak stress [5, 20]. In Fig. 10(b), the relation between σ_1 and σ_3 is shown. In accordance with linear Mohr-Coulomb criterion, we can obtain the strength parameters of flawed coarse marble, which is listed in Table 3.

In accordance with Table 3, it can be seen that the values of C and φ are respectively 22.14 MPa and 28.0° for intact coarse marble; while the values of C and φ are respectively 20.76 MPa and 30.4° for flawed coarse marble by different samples except for four samples (C15$^{\#}$, C22$^{\#}$, C24$^{\#}$ and C26$^{\#}$), which shows only ~10% difference between intact and flawed coarse marble. However the values of C and φ are respectively 19.95 MPa and 31.2° for flawed coarse marble under Path III (10 MPa$\leq\sigma_3\leq$30 MPa), which is approximately equal with that for flawed coarse marble by different samples. The above conclusion testifies the feasibility and accuracy to confirm the cohesion and internal friction angle of rock by Path III with only one sample.

Figure 10(c) presents the relation between the confining pressure and circumferential strain of flawed coarse marble under Path III. During increasing the hydrostatic stress ~*oa*, the circumferential deformation equals to zero approximately. And then the σ_3 is maintained a constant level, the axial deviatoric stress is increased until post-peak stress "*c* point" at a constant displacement rate of 0.002 mm/s. It needs to notice that corresponding axial strain of *c* point is a little higher than peak axial strain. During increasing axial deviatoric stress ~*ac*, the circumferential deformation increases gradually. Finally, while the axial deformation is maintained constant ~6.44×10^{-3}, the σ_3 is reduced from 30 MPa at a rate of 0.1 MPa/s. During reducing the confining pressure ~*cd*, the axial stress also decrease gradually, but the circumferential deformation increases rapidly. Due to local behavior in the process ~*cd*, the initial elastic deformation will transfer the plastic deformation on

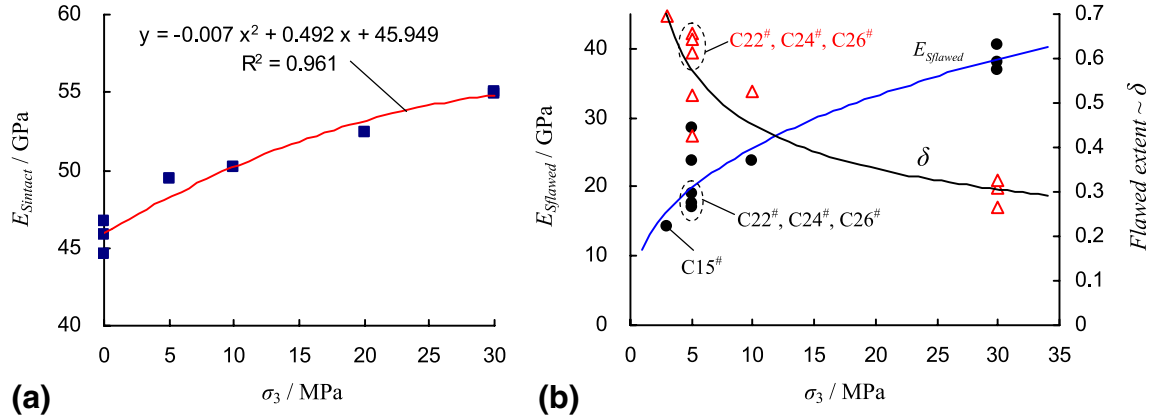

Fig. 9 Elastic modulus of intact and flawed coarse marble under different confining pressures, and the flawed extent of flawed coarse marble under different confining pressures

the yielding surface. The increase of circumferential deformation is closely related to the axial plastic deformation, which shows that the failure of rock sample results from the rapid increase of circumferential deformation.

The failure mode of flawed coarse marble under Path III is shown in Fig. 10(d). It is very clear that the flawed coarse marble takes on a typical shear failure and the fracture surface is very smooth, which is similar with that of intact marble at lower confining pressure shown in Fig. 5. Therefore the failure of flawed coarse marble under Path III is essentially the state transition from the plastic state to brittle state. The failure of confining pressure reduction is actually the occurrence of brittle fracture of rock. However the coarse marble takes on more ductile failure while loading continuously for the rock under triaxial compression.

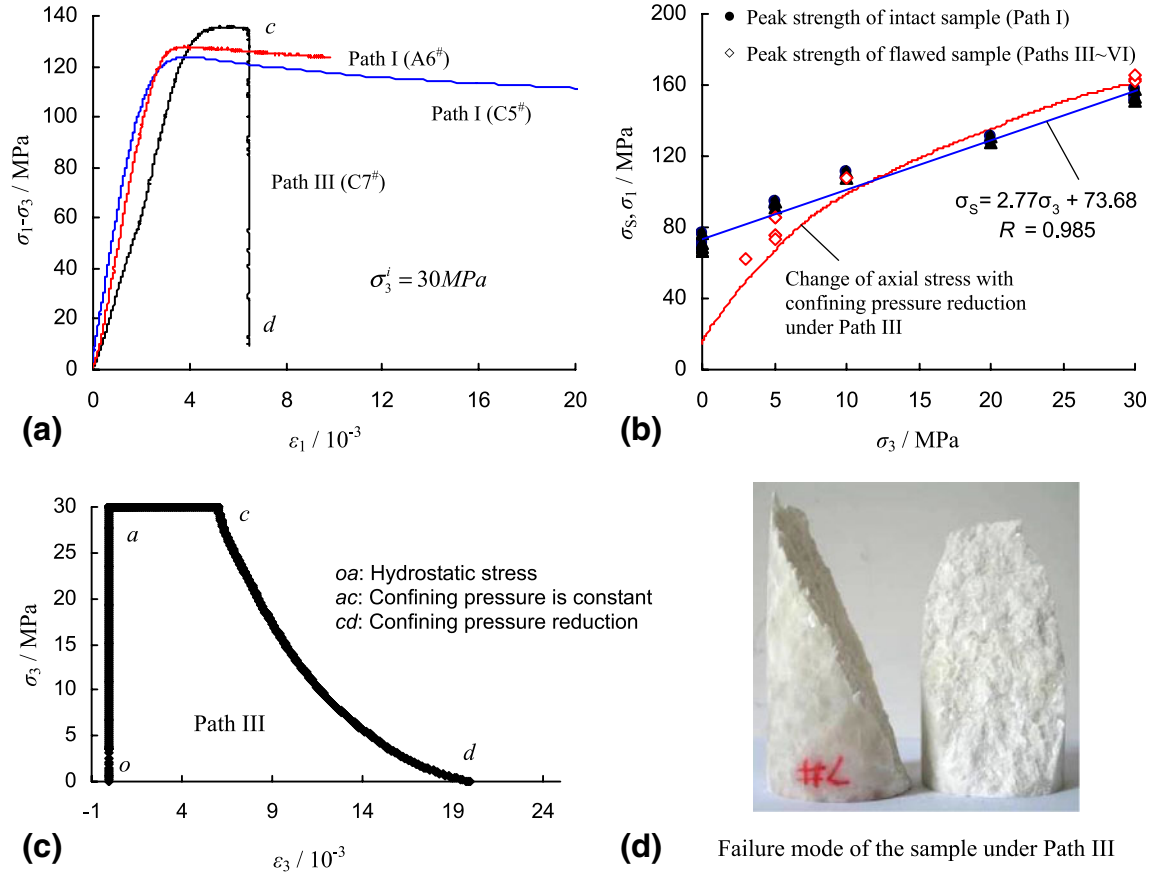

Fig. 10 Triaxial experiment results of flawed coarse marble under Path III

Table 3 Strength parameters of flawed coarse marble in accordance with linear Mohr-Coulomb criterion

Sample	Loading path	σ_0 / MPa	q	R	C/MPa	φ /(°)	Note
Intact coarse marble	I	73.68	2.77	0.985	22.14	28.0	With UCS
Flawed coarse marble	III~VI	72.52	3.05	0.995	20.76	30.4	Different samples expect for four samples (C15#, C22#, C24# and C26#)
Flawed coarse marble	III	70.81	3.15	0.995	19.95	31.2	One sample (10 MPa≤σ_3≤30 MPa)

Re-fracture Mechanical Behavior of Flawed Sample Under Different Loading Paths (Path IV and V)

Figure 11 shows axial stress-axial strain curves of flawed coarse marble under Path IV, and the corresponding re-fracture strength and deformation parameters are presented in Table 4. The ~E_S is defined as elastic modulus, i.e. the slope of approximation linear part in the axial stress-axial strain curve. The ~ε_{1c} represents the axial strain value at rupture in terms of axial stress-axial strain curve of flawed coarse marble under final confining pressure (σ_3=0 MPa). The ~E_{50} represents the deformation modulus, i.e. the slope between the original point and the axial deviatoric stress at an half of TCS.

From Fig. 11, it can be seen that the mechanical behavior of two flawed coarse marble samples at $\sigma_3^i = 30$MPa have better consistency before unloading, which can be used to investigate the effect of post-peak damage extent on the re-fracture mechanical behavior of flawed coarse marble in uniaxial compression. At $\sigma_3^i = 30$MPa, the C14# sample is unloaded after the post-peak axial strain ~6.55×10^{-3}, while the C27# sample is unloaded after the post-peak axial strain ~13.03×10^{-3}. From the unloading curve, we can see that the C27# sample has larger plastic deformation than C14# sample, which results from the larger compressed post-peak axial deformation of C27# sample.

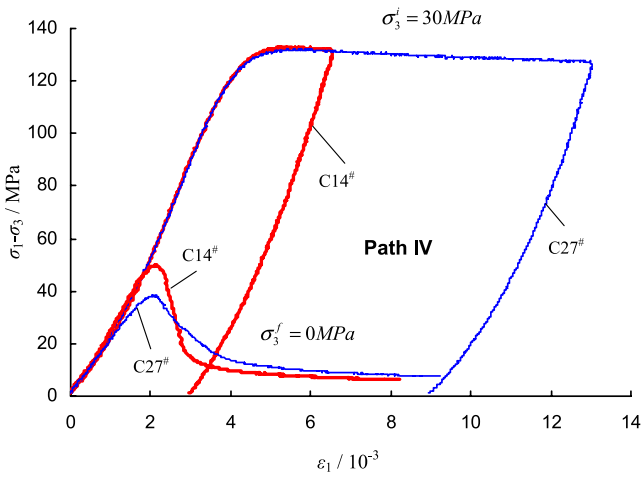

Fig. 11 Re-fracture axial stress-axial strain curves of flawed coarse marble under Path IV

In accordance with Table 4, we can see out that the peak strength and Young's modulus of damage samples (compressed until post-peak stress at $\sigma_3^i = 30$MPa) are all lower compared with that of intact sample; moreover the peak strength and Young's modulus of damage samples C27# are lower for the larger compressed post-peak plastic deformation of coarse marble, which results from more serious damage of C27# sample with larger compressed deformation. However the peak axial strains of two samples are approximately equal, which is not dependent to the flawed or damage extent in the rock. Besides, in final uniaxial compression, the C27# sample takes on more plasticity after peak strength than C14# sample.

Under Path IV, final failure modes of flawed coarse marble are shown in Fig. 12. In order to compare, the failure mode of intact sample under uniaxial compression (Path I) is also presented in Fig. 12. From Fig. 12, it can be found that the intact and flawed coarse marble all take on typical shear failure mode. However, the failure mode of flawed coarse marble under Path IV is a shear zone as shown in the ellipticity of Fig. 12, which is more complicated than that (a shear plane) of intact coarse marble under Path I. Nearby the main shear zone, there are a lot of minute and dense cracks, which shows that the flawed sample takes place a certain of damage after compressed to the post-peak stress at $\sigma_3^i = 30$MPa. Moreover the sample has more serious damage for the larger axial compressive deformation, and thus the irrecoverable plastic deformation of this sample is larger after unloading. After the σ_3 is adjusted to zero, the stress state of rock changes into 1-D (one-dimensional) from 3-D, which results in the complexity of failure mode for damage sample (Fig. 12).

Under Path V, Fig. 13 shows axial stress-axial strain curves of flawed coarse marble under initial and final confining pressures. The corresponding re-fracture strength and deformation parameters of flawed coarse marble under different loading paths are listed in Table 5. It is very clear that under initial different confining pressures three samples are loaded to the same post-peak strain ~9.8×10^{-3} and then are unloaded to zero at a rate of 2×10^{-5}/s. From Fig. 13, it can be seen that the post-peak deformation of fractured rock changes from softening to hardening with the increase of σ_3, which tends towards the stable state from unstable state after post-peak stress. At $\sigma_3^f = 30$MPa, three damage samples

Table 4 Re-fracture strength and deformation parameters of flawed coarse marble under Path IV

Sample	Loading path	σ_3^f/MPa	σ_S^f/MPa	ε_{1c} / 10^{-3}	E_S / GPa	E_{50} / GPa	Note
C35#	I	0	67.21	1.841	45.82	37.37	Intact sample
C14#	IV	0	49.94	2.118	27.14	25.24	Damage sample
C27#	IV	0	38.37	2.074	20.28	21.53	Damage sample

compressed until post-peak stress under initial confining pressures all have distinct yielding platform, which takes on ideal plasticity. Moreover we can conclude that the relation between axial deviatoric stress and deformation of fractured coarse marble is almost in-dependent to the heterogeneous difference among three flawed coarse marble samples and the previous loading history, which shows that the maximum supporting capacity and elastic modulus of fractured coarse marble is not related to the fractured extent. The friction among crystal grains determines the strength behavior of damage coarse marble. From Fig. 14, the friction slippage is clearly visible, which further validates the fractured coarse marble can support higher axial loads than its material strength by friction. The total deformation in fractured coarse marble tends to uniform and then appears ideal plasticity.

In accordance with Table 5, compared with the flawed sample, the damage sample failed with lower peak strength, a little smaller elastic moduli, and larger failure strains. However the deformation modulus of damage sample is a little higher than that of flawed sample, which results from more increase of initial stiffness for damage sample than flawed sample. For damage sample, under higher confining pressures (σ_3=30 MPa), the axial supporting capacity and elastic modulus of damage coarse marble is not related to the loading path, while the deformation modulus and peak strain of damage sample depend on the difference of initial confining pressure. If the initial confining pressure is lower, the peak axial strain and deformation modulus is also smaller.

Figure 14 shows the failure modes of flawed coarse marble under Path V. From Fig. 14, we can conclude that all flawed coarse marble takes on the shear failure with a single plane, and the fracture surface is very smooth. After peak stress, the flawed coarse marble takes on the friction slippage between two blocks. With the increase of confining pressure from σ_3^i to σ_3^f, two fractured blocks begin to close and support higher axial stress by friction. Figure 15 shows the comparison on axial stress-axial strain curves between intact sample, flawed sample and damage sample. It is very clear that axial supporting capacity of damage sample tends towards ideal plasticity, while intact and flawed sample firstly comes out a peak stress, and then with the increase of axial deformation, the axial supporting capacity of intact and flawed sample decreases slowly towards the residual strength. Moreover damage sample has more non-linear plastic deformation after yielding stress than intact or flawed sample.

Re-fracture Mechanical Behavior of Flawed Sample Under Path VI

In order to investigate the weakening of peak strength of fractured rock and the difference of strength parameters obtained by various loading paths, the re-fracture mechanical experiments of flawed coarse marble under Path VI were carried out under different confining pressures. Under Path VI, the sample was applied to the same axial strain ~9.8×10^{-3} and then the axial deviatoric stress was not unloaded; while under Path V, the sample was loaded to post-peak axial strain ~9.8×10^{-3} and then the axial deviatoric stress was unloaded to zero. The detailed difference can be found in Figs. 1 and 2.

Figure 16 shows triaxial stress-strain curves of flawed coarse marble under Path VI. In Fig. 16, when the sample is loaded until post-peak control point *h*, a larger stress drop comes out, i.e. the axial stress reduces a lot while the axial

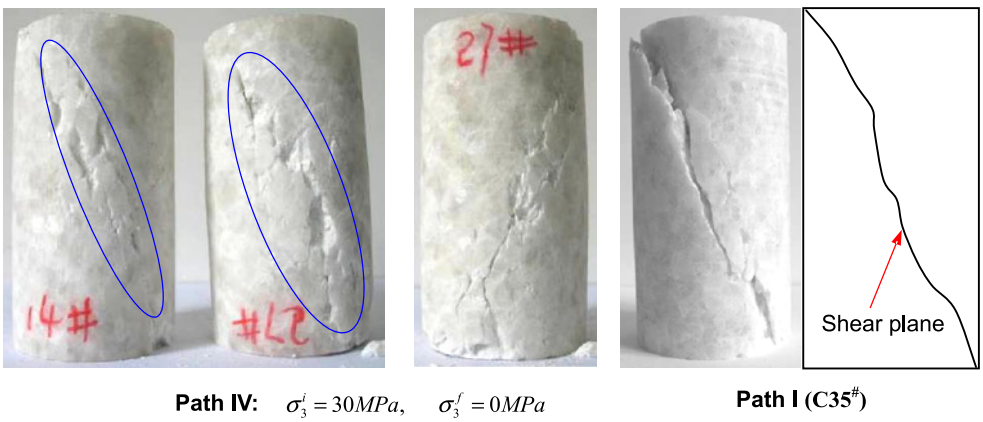

Fig. 12 Final failure modes of flawed coarse marble under Path IV. The failure mode of intact sample under uniaxial compression (Path I) is also shown in this figure

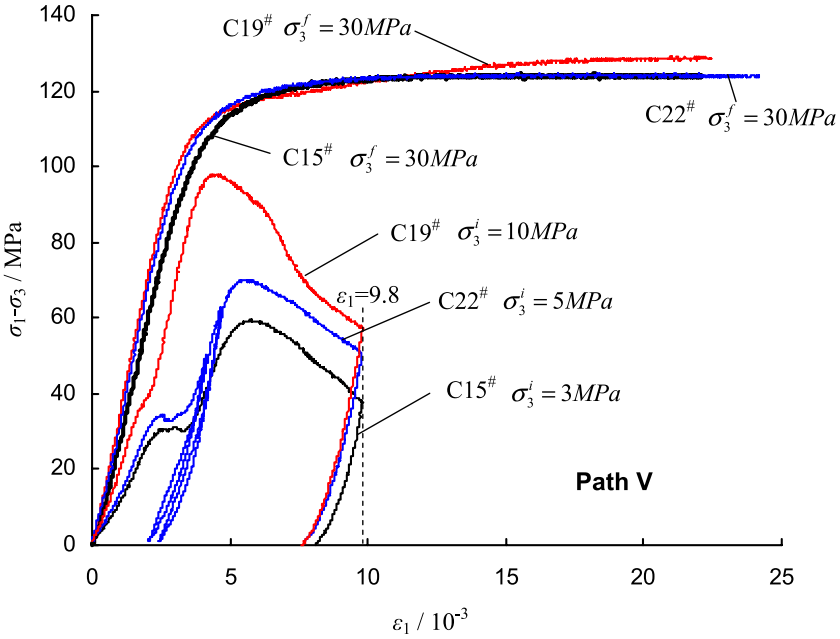

Fig. 13 Re-fracture axial stress-axial strain curves of flawed coarse marble under Path V. The damage coarse marble was defined to the flawed sample compressed until post-peak stress, and then which is unloaded in order to investigate the re-fracture behavior of flawed coarse marble under higher confining pressure of 30 MPa

strain is constant, which results from the stress relaxation of adjusting the parameter to increase the σ_3. In terms of Fig. 16, damage sample compressed under initial confining pressure has better yielding platform, which shows ideal plasticity even though under lower confining pressure of 10 MPa. The re-fracture deformation behavior is distinctly different from the softening characteristics of flawed coarse marble as shown in Fig. 8 at σ_3=10 MPa.

The above analysis shows that it is necessary to take into account whether rock engineering is the fractured rock mass or not when carrying out the numerical simulation for engineering rock mass in practice. We cannot make the numerical analysis by a simple strain-softening model of rock. Only by looking for the constitutive model adapted to different stress states of rock mass, the calculated results would be able to approach the rock engineering practice. The fractured rock mass is in essence a non-continuous medium, but which is closer to the behavior of a continuous medium under higher confining pressures. Therefore it may be more convenient to investigate the problem of non-continuous medium by adopting the method of continuous media under higher triaxial stress states.

In Fig. 16(a), the axial stress-axial strain curve of the sample C26# has great difference compared with other two samples at $\sigma_3^i = 5$MPa, which causes the following problem. Whether the re-fracture mechanical test results of damage samples compressed for flawed samples with different flawed extents can be used to investigate the weakening of peak strength of fractured rock or not ? To explain this above problem, the experimental results of two flawed sample at the same confining pressure are presented in Fig. 16(b). From Fig. 16(b), it can be seen that the axial supporting capacity of two damage samples at $\sigma_3^f = 20$MPa are approximately equal with the difference only 1.69 MPa although the strength and deformation behavior of two flawed samples are distinctly different at $\sigma_3^i = 5$MPa. Therefore, the experimental results shown in Fig. 16 can be used to analyze the strength parameters of flawed and damage coarse marble obtained by different loading paths, which is presented in Fig. 17.

From Fig. 17, it is very clear that the sensitivity of the peak strength of damage sample on the confining pressure is higher than that of flawed sample on the confining pressure. Flawed sample under initial lower confining pressure was compressed until after post-peak stress, which formed the

Table 5 Re-fracture strength and deformation parameters of flawed coarse marble under different loading paths

Sample	Loading path	σ_3 / MPa	σ_S / MPa	ε_{1c} / 10^{-3}	E_S / GPa	E_{50} / GPa	Note
C7#	III	30	165.97	5.246	40.39	30.91	Flawed sample
C27#	IV	30	162.22	6.015	37.00	27.64	Flawed sample
C14#	IV	30	163.19	5.203	37.88	27.99	Flawed sample
C15#	V	30	154.52	15.55	31.97	29.55	Damage sample
C22#	V	30	154.70	16.91	36.07	33.19	Damage sample
C19#	V	30	159.16	22.00	36.68	35.30	Damage sample

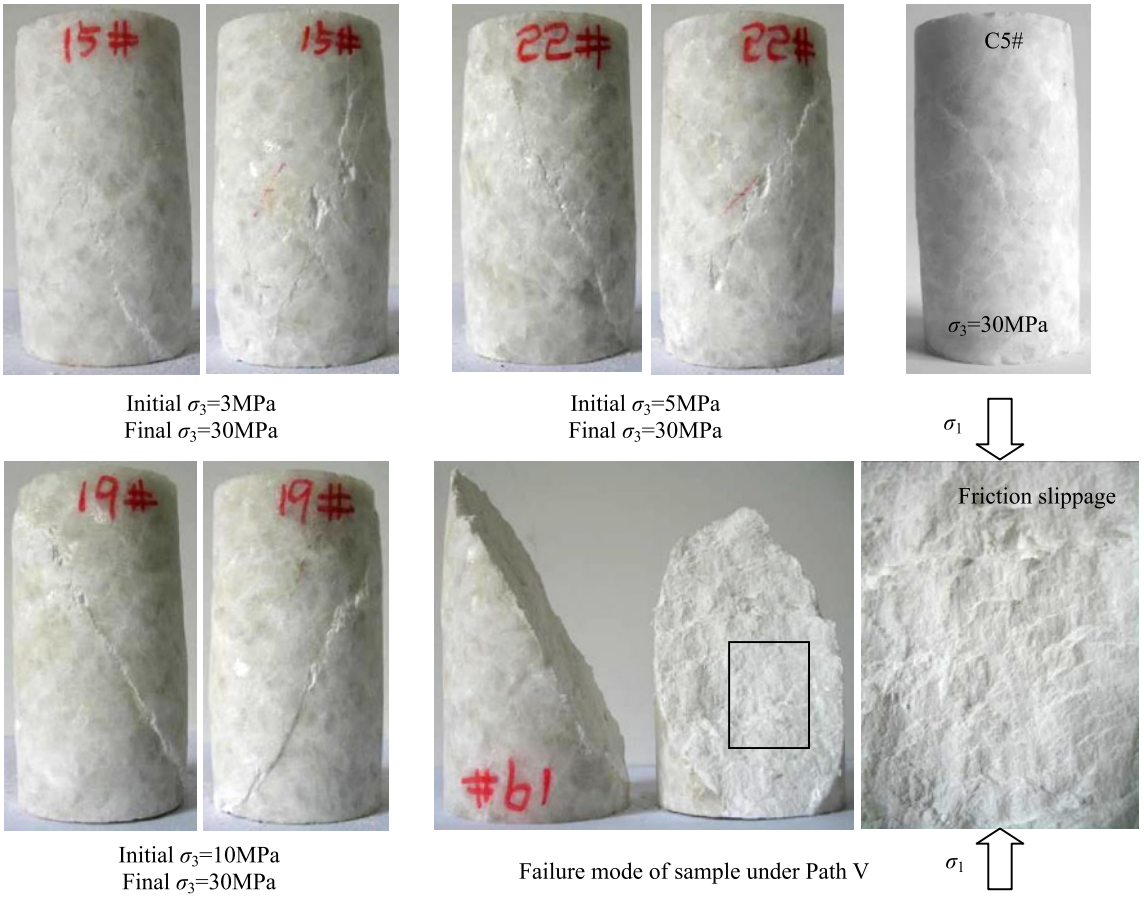

Fig. 14 Failure modes of flawed coarse marble under Path V

damage sample. At this time, the macroscopic failure surface has come out in the damage sample. Therefore under higher confining pressure, the damage sample supports the axial deviatoric stress only by friction among fracture surfaces. In accordance with Fig. 17, it is clear that σ_0 equals to 72.52 and 48.11 MPa for flawed and damage coarse marble, respectively. However q is 3.05 and 3.58 for flawed and damage coarse marble, respectively. According to equations (1) and (2), the values of cohesion (C) and internal friction angle (φ) calculated for intact, flawed and damage samples under different loading paths are presented in Table 6. From Table 6, it can be seen that the value of C for flawed coarse

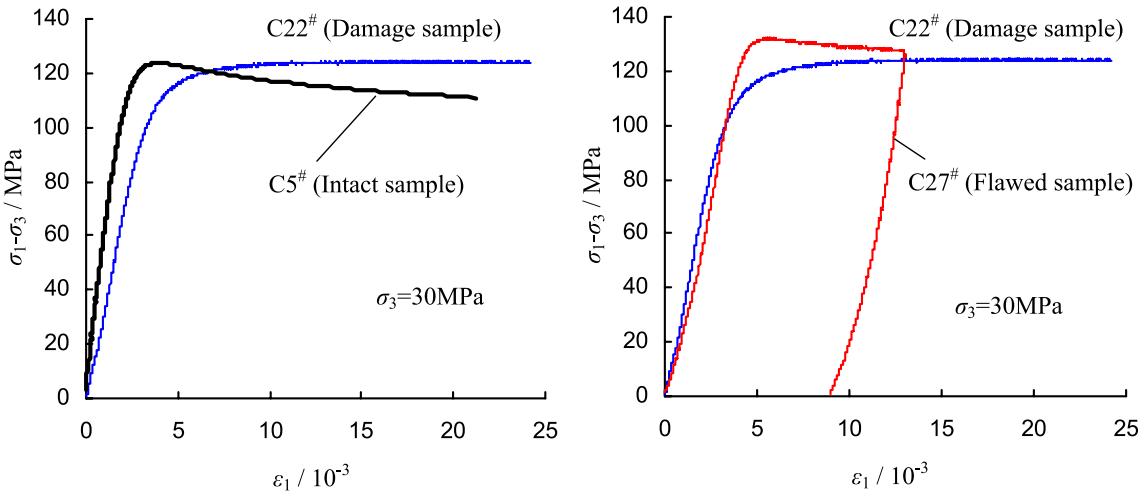

Fig. 15 Comparison on axial stress-axial strain curves between intact sample, damage sample and flawed sample

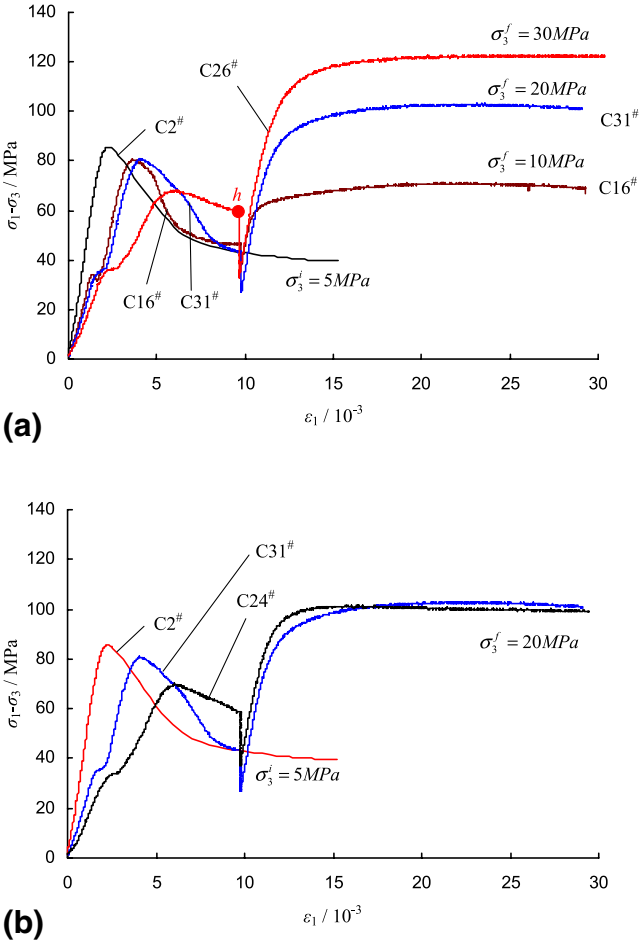

Fig. 16 Triaxial stress-strain curves of flawed coarse marble under Path VI

marble equal to 20.76 MPa, while the value of φ are 30.4°. However, the value of C of damage coarse marble equals to 12.71 MPa, while the value of φ is 34.3°. Therefore, the value of C of damage sample is lower than that of flawed sample, but the value of φ of damage sample is higher than that of flawed sample.

According to Fig. 17, the influence of loading path on peak strength of coarse marble can be concluded. With the increase of σ_3, the difference of peak strength between flawed and damage sample tends to decrease. At σ_3=10 MPa, the peak strength of damage sample is lower ~26.66 MPa than that of flawed sample. However at σ_3=30 MPa, the peak strength of flawed and damage sample is approximately equal, which shows no significant effect of loading path on the flawed coarse marble under this confining pressure. Moreover from Fig. 17, we can predict approximately that beyond σ_3= 30 MPa, the peak strength of flawed and damage coarse marble may be independent of the loading path.

Figure 18 shows failure modes of flawed coarse marble under Path VI. At σ_3^f = 10MPa, the flawed coarse marble leads to typical shear failure mode with a single fracture surface and the fracture angle is about 63° with the direction of σ_3. At σ_3^f = 20MPa, two flawed coarse marble all lead to typical shear failure mode with a single fracture surface, but the fracture angle of sample C24# is about 55°, which is a littler lower than that of the sample C31# (60°). Moreover despite the above two samples has single shear failure mode, the sample C24# is more complicated than the sample C31#, which possesses double slippage planes in the sample C24#. At σ_3^i = 5MPa, the sample C24# has taken on shear failure after being loaded to post-peak stress. At the time, when the confining pressure is adjusted to 20 MPa, the increase of axial deformation makes the internal material in the sample happen the yielding fracture from lower strength to higher strength, which results in new failure surface. Therefore two surfaces in the sample C24# take place yielding step by step. However at σ_3^f = 30MPa, the flawed coarse marble shows typical conjugate shear failure and takes on drum. From the local magnification of C26#, we can see that the sample possesses conjugate shear failure characteristics and the fracture angle is approximately 45~50°.

Figure 19 shows typical friction slippage of flawed coarse marble under higher confining pressures. From Fig. 19, we can see that the friction slippage is very visible. Compared with that of the sample C19# shown in Fig. 14, the two samples in Fig. 19 lead to shear failure mode with a single fracture surface. But the two samples in Fig. 19 takes on a little cone shear failure, not a complete plane shear failure of the sample C19# shown in Fig. 14. Moreover the two samples in Fig. 19 take on the failure behavior with step shape. Although the final confining pressure of the samples C16# and C31# are different, the fracture surface and slippage behavior of two samples are almost completely similar, which further validates that the fractured sample supports the axial stress by friction.

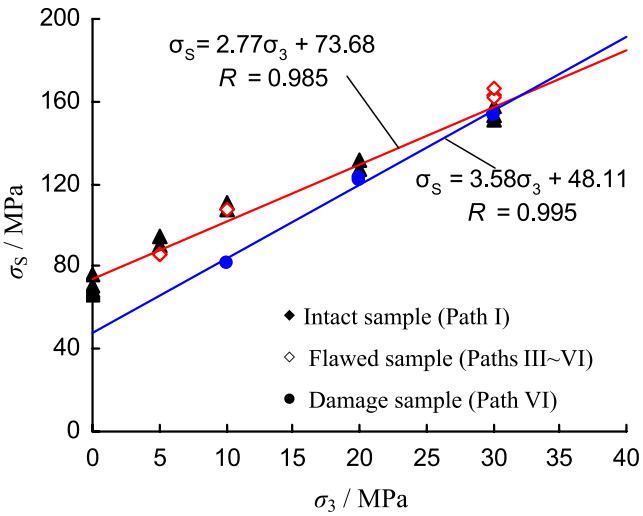

Fig. 17 Relation between peak strength and the confining pressure of flawed and damage coarse marble under different loading paths

Table 6 Re-fracture strength parameters of flawed and damage coarse marble under different loading paths

Sample	Loading path	σ_0 / MPa	q	R	C/MPa	φ /(°)	Note
Flawed coarse marble	III~VI	72.52	3.05	0.995	20.76	30.4	Different samples
Damage coarse marble	VI	48.11	3.58	0.995	12.71	34.3	N/A

The effect of two loading paths (Path IV and VI) on the complete stress-strain curves of flawed coarse marble is presented in Fig. 20. The circumferential deformation was measured by circumferential LVDT. From Fig. 20, it can be seen that two damage coarse marble samples compressed until post-peak stress all have distinct circumferential plastic strain. If not taking into account initial circumferential plastic strain, we can see that the circumferential strain of damage sample is smaller at the stages of crack closure and elastic deformation (i.e. before the round dot), which is almost inappreciable compared that after peak strength. At the stage of deformation localization, the circumferential strain of damage sample increases rapidly with the axial strain, which results from that the circumferential strain of damage sample after yielding stress reflect sensitively the yielding and softening process of internal material in the rock. However after a point, with the increase of axial strain, the circumferential strain of damage sample increases linearly, which can be explained as follows. The damage sample supports the axial stress only by friction. Moreover we can conclude that the increasing coefficient k ($k=\varepsilon_3/\varepsilon_1$) of circumferential strain with axial strain is completely equal, which shows no effect of loading path on the coefficient k of damage sample, and further testifies the supporting by friction slippage. It needs to be noticed that the circumferential strain of damage sample after A point is parallel with the axial strain, which results from the circumferential deformation has reached the maximum measurement range of circumferential LVDT, therefore the circumferential strain after A point can not reflect actually circumferential deformation behavior of flawed coarse marble.

Conclusions

An experimental investigation on the strength, deformation and failure behavior of coarse marble under six different loading paths was carried out. Based on the experimental results of coarse marble samples under various loading paths, the following conclusions can be drawn.

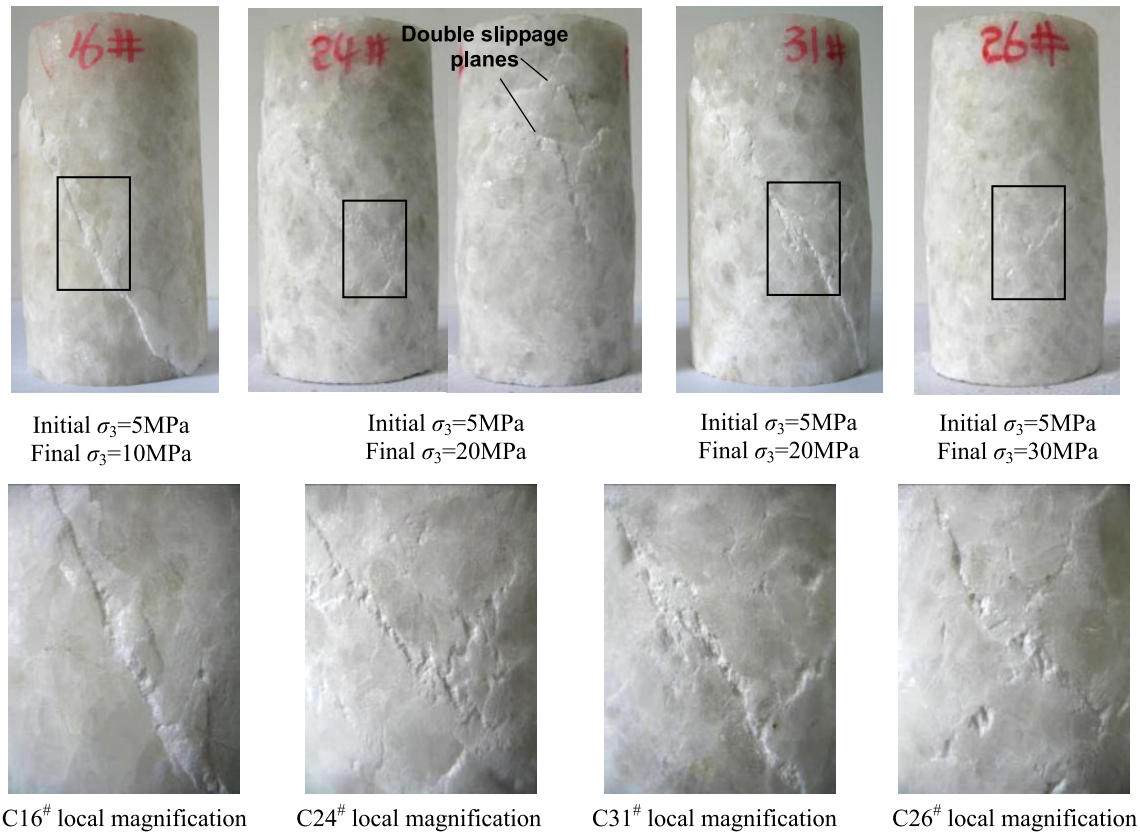

Fig. 18 Failure modes of flawed coarse marble under Path VI

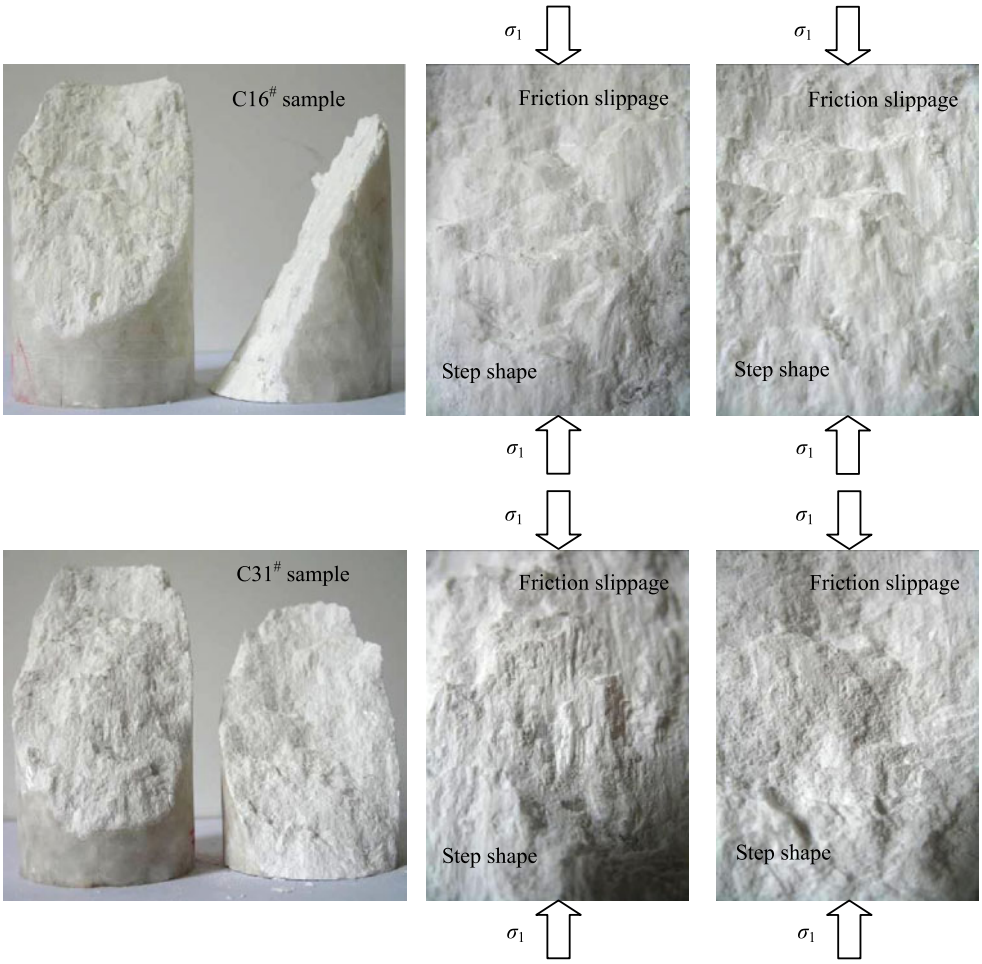

Fig. 19 Typical friction slippage of flawed coarse marble under higher confining pressures

Loading path has a significant effect on the strength, deformation and failure behavior of coarse marble under triaxial compression. In present study, tested coarse marble is a kind of typical plastic and ductile rock material and takes on typically shear failure mode even though in uniaxial compression. With the increase of confining pressure, the post-peak deformation of coarse marble changes gradually from brittleness to ductility. Flawed samples fail with smaller Young's moduli and larger failure strains compared with intact samples at the same confining

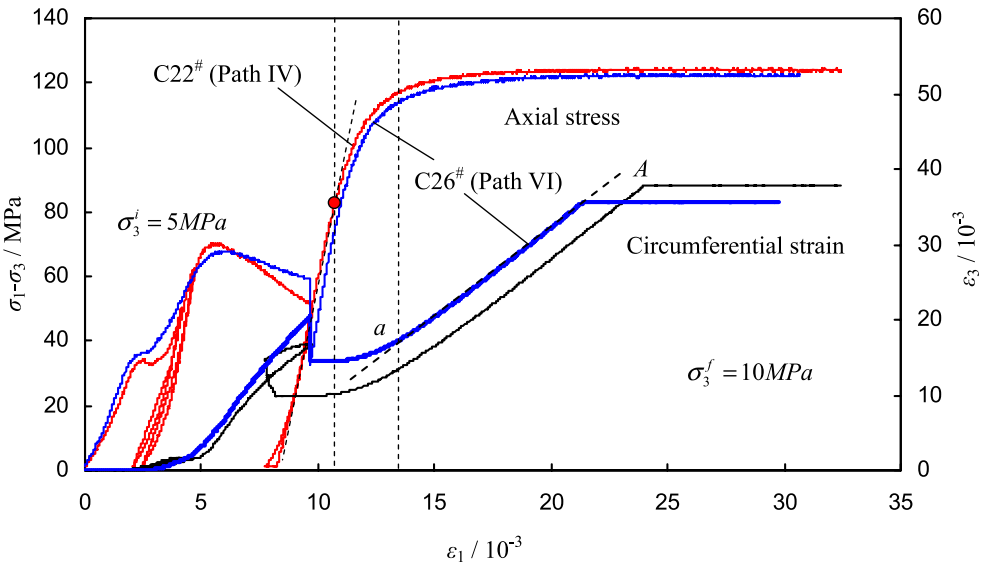

Fig. 20 Effect of loading path on the complete stress-strain curves of flawed coarse marble

pressure. Under lower confining pressures (≤10 MPa), all the axial stress-axial strain curves of flawed samples show a turning point (an abrupt change of slope) at the deviatoric stress of about 35 MPa, coincident with local yield in the coarse marble. But with the increase of σ_3, this turning point at the deviatoric stress of about 35 MPa will decrease step by step.

Confining pressure has different effect on the strength difference between intact and flawed sample. Under lower confining pressures (e.g. 5 MPa), the peak strength of flawed sample is lower than that of intact sample. Under medium confining pressures (e.g. 10 MPa), the peak strength of flawed sample is approximately equal to that of intact sample. However under higher confining pressures (e.g. 30 MPa), the peak strength of flawed sample is higher than that of intact sample. The above conclusion can be explained as follows. With the increase of σ_3, the local yield will take place in advance. And thus the material in the rock extrudes and fractures after local yield, which fills in the internal voids of flawed sample and strengthens the supporting structure in the rock material. But with the increase of σ_3, this kind of strengthening will become more and more distinct, which can increase the elastic modulus of flawed sample after turning point, as shown in Fig. 8(c). Therefore the difference on peak strength of between flawed and intact sample increases with the increase of σ_3.

Three loading paths (Paths I–III) are put forward to confirm the strength parameters (cohesion and internal friction angle) of coarse marble in accordance with linear Mohr-Coulomb criterion. Compared among the strength parameters, two loading paths (i.e. Path II by stepping up the confining pressure and Path III by reducing the confining pressure after peak strength) are suggested to confirm the triaxial strengths of rock under different confining pressures by only one sample, which is very applicable for a kind of rock that has obvious plastic and ductile deformation behavior (e.g. marble, chalk, mudstone, etc.).

In order to investigate re-fracture mechanical behavior of rock material, three loading paths (Paths IV–VI) are also put forward for flawed coarse marble. The peak strength and deformation failure mode of flawed coarse marble are found depending on the loading path (Paths IV–VI). Under lower confining pressures, the peak strength and Young's modulus of damage samples (compressed until post-peak stress under higher confining pressure) are all lower compared with that of flawed sample; moreover mechanical parameters of damage samples are lower for the larger compressed post-peak plastic deformation of coarse marble. However under higher confining pressures (e.g. σ_3= 30 MPa), the axial supporting capacity and elastic modulus of damage coarse marble (compressed until post-peak stress under lower confining pressure) is not related to the loading path, while the deformation modulus and peak strain of damage sample depend on the difference of initial confining pressure and post-peak plastic deformation. The friction among crystal grains determines the strength behavior of flawed coarse marble under different loading paths.

In the range of tested final confining pressures, the sensitivity of the peak strength of damage sample on the confining pressure is higher than that of flawed sample on the confining pressure, which results in that the value of cohesion of damage sample is lower than that of flawed sample, but the value of internal friction angle of damage sample is higher than that of flawed sample.

Acknowledgments This project is supported by the National Natural Science Foundation of China (no. 50709008), which is greatly appreciated. We would also like to acknowledge the editors and two anonymous reviewers for their valuable comments, which have greatly improved this paper.

References

1. Jaeger JC (1967) Brittle fracture of rocks. Proceedings of eighth symposium on rock mechanics. Port City, Baltimore, pp 3–57
2. Swanson RS, Brown WS (1971) An observation of loading path independence of fracture in rock. Int J Rock Mech Min Sci 8 (3):277–281
3. Crouch SL (1972) A note on post-failure stress-strain path dependence in Norite. Int J Rock Mech Min Sci 9(2):197–204
4. Xu DJ, Geng NG (1986) The various stress paths causing deformation and failure in rocks. Rock Soil Mech 7(2):17–25
5. Wang B, Zhu JB, Wu AQ et al (2008) Experimental study on mechanical properties of Jinping marble under loading and unloading stress paths. Chin J Rock Mech Eng 27(10):2138–2145
6. Gen NG (1982) Volume changes of rocks in various stress paths. Northwest Seismol J 4(1):115–124
7. Yao XX, Geng NG, Chen Y (1980) The effect of stress path on brittleness and ductility of rocks. Acta Geophys Sin 23(3):312–319
8. Shen MY, Shi ZM, Zhang L (2003) Deformation properties of samples under different loading paths. Chin J Rock Mech Eng 22 (8):1234–1238
9. Xiong SH, Zhou HM (2006) Deformation properties of rock mass of TGP permanent shiplock slopes under complex stress paths. Chin J Rock Mech Eng 25(Supp.2):3636–3641
10. Lee DH, Juang CH, Chen JW et al (1999) Stress paths and mechanical behavior of a sandstone in hollow cylinder tests. Int J Rock Mech Min Sci 36:857–870
11. Yang CH, Bai SW, Wu YM (2000) Stress level and loading path effect on time-dependent properties of salt rock. Chin J Rock Mech Eng 19(3):270–275
12. Ferfera FMR, Sardau JP, Bouteca M et al (1997) Experimental study of monophasic permeability changes under various stress paths. Int J Rock Mech Min Sci 34(3–4):413, paper No. 037
13. Cai M (2008) Influence of stress path on tunnel excavation response—Numerical tool selection and modeling strategy. Tunn Undergr Space Technol 23:618–628
14. Lavrov A (2001) Kaiser effect observation in brittle rock cyclically loaded with different loading rates. Mech Mater 33:669–677
15. Chen Y (1979) Acoustic emission of rocks under triaxial compression with various stress paths. Intern Int J Rock Mech Min Sci & Geomechanics Abstr 16(6):401–405

16. Su CD, Gao BB, Nan H, Li XJ (2009) Experimental study on acoustic emission characteristics during deformation and failure processes of coal samples under different stress paths. Chin J Rock Mech Eng 28(4):757–766
17. Xiang TB, Feng XT, Chen BR, Jing Q (2008) True triaxial and acoustic emission experimental study of failure process of hard rock under excavating and supporting stress paths. Rock Soil Mech 29(Supp):500–506
18. Li YH, Yuan RF, Zhao XD (2007) Effect of different stress paths on Kaiser Effect of rock acoustic emission. J Northeast Univ Nat Sci 28(4):576–579
19. Yao XX (1981) Observation of micro-cracks within gabbro in experiments along various stress paths. Acta Geophys Sin 3(1):49–54
20. Zhang HB, Song XG, Huang MS, Shang QS (2007) Research on failure features of rocks under different stress unloading path. J Shandong Univ Eng Sci 37(6):83–86
21. Yang SQ, Jiang YZ, Xu WY, Chen XQ (2008) Experimental investigation on strength and failure behavior of pre-cracked marble under conventional triaxial compression. Int J Solids Struct 45(17):4796–4819
22. Han LJ, Yang MJ (2009) Re-fracture process and mechanical characteristics of cracked rock samples. Int J Rock Mech Min Sci 46:738–747
23. Yang SQ, Dai YH, Han LJ et al (2009) Experimental study on mechanical behavior of brittle marble samples containing different flaws under uniaxial compression. Eng Fract Mech 76(12):1833–1845
24. Fairhurst CE, Hudson JA (1999) Draft ISRM suggested method for the complete stress-strain curve for the intact rock in uniaxial compression. Int J Rock Mech Min Sci 36:279–289
25. Yang SQ, Su CD, Xu WY (2005) Experimental and theoretical study of size effect of rock material. Eng Mech 22(4):112–118
26. Yang SQ, Su CD, Xu WY (2005) Experimental investigation on strength and deformation properties of marble under conventional triaxial compression. Rock Soil Mech 26(3):475–478